PERFORMANCE OF A SMALL-COMPACT X-MP RADAR TO MONITOR EXTREME RAINFALL EVENT ON 7 JULY 2018

MAGFIRA SYARIFUDDIN
Earth Observatory of Singapore, Asian School of the Environment, Nanyang Technological University, Singapore, Singapore, magfira.syarifuddin@ntu.edu.sg
State Agriculture Polytechnic of Kupang, Kupang, Indonesia.

MARIKO OGAWA
Center for South East Asia, Kyoto University, Kyoto, Japan, ogwmari@cseas.kyoto-u.ac.jp

HARUHISA NAKAMICHI
Disaster Prevention Research Institute, Kyoto University, Kagoshima, Japan, nakamiti@svo.dpri.kyoto-u.ac.jp

SATORU OISHI
Research Centre for Urban Safety and Security, Kobe University, Kobe, Japan, tetsu@phoenix.kobe-u.ac.jp

MASATO IGUCHI
Disaster Prevention Research Institute Kyoto, University, Kagoshima, Japan, iguchi.masato.8m@kyoto-u.ac.jp

ABSTRACT

Japan experienced a breaking-record rainfall event from Western Japan to the Tokai region from 28 June to 8 July 2018. This paper analyzes the peak rainfall of this event on 6-8 July 2018 in Kagoshima by a small-compact X-band Multi-Parameter (MP) radar. The aim of this paper is to know the reliability of the rain rate estimated by the radar during the extreme rainfall event. The estimated rain rate provided by the X-MP radar using an unknown algorithm (Furuno) is compared to three different radar algorithms based on radar reflectivity factor (Z_H), specific differential phase shift (K_{DP}), and differential reflectivity (Z_{DR}). The estimated radar-based rain rate at 500m height is then compared to the ground-based rain measured by a rain gauge. The K_{DP}-Z_H -based rain algorithm gives the closest values to the unknown Furuno algorithm, which indicates the use of K_{DP} parameter as the rain rate estimator. The spatial information of radar is able to monitor more than 250 mm rain depth, which cannot be obtained by the rain gauge. In general, the point-based comparison between hourly radar-based rain rate and ground-based rain rate shows a similar temporal fluctuation, but in general, most of the values on 7 July 2018 fall below the rain gauge measurement. The estimated Furuno rain rate and the Z_{HH}-K_{DP} -based algorithm gives the closest values to the increase of ground-based rain depth at 1:0.94 and 1:0.89 ratios, respectively, while the Z_{HH}-Z_{DR} -based algorithm has the lowest ratio of 1:0.79.

Keywords: X-MP radar, radar-based rain rate estimate, the heavy rain of July 2018, Kagoshima

1. INTRODUCTION

Accurate spatial and temporal measurement of rain is important for hydrology, disaster mitigation, and water resources management. A rain gauge, which is the most traditional rain instrument, is cheaper but offers limited information on the spatial rainfall variability over a larger area, such as a watershed (Ciach and Krajewski, 2016). The weather radars have become the most appealing instruments that can measure areal precipitation with both a high spatial and temporal resolution.

Depending on the operational wavelength, the spatial resolution offered by a weather radar system can range from tens meters to several kilometers, within seconds to days temporal resolution. Most of weather radars are operated at S-band and C-band wavelength, which do not suffer from attenuation but give a coarser spatial and temporal resolution. Recently, the X-band radar has gained more attention in hydrology and meteorology, as it can measure higher spatial resolution with only a small antenna. The new development in the X-band radar is the dual polarimetric, which not only measures the reflectivity intensity (Z_H) and the Doppler information (Doppler velocity, V_D and Doppler velocity spectrum width, σ_{VD}) but also multi-parameter (MP) information. The MP allows a better insight into the rain and a far more reliable quantitative precipitation estimate (QPE) (Bringi and Chandrasekar, 2001; Park et al., 2005; Doviac and Zrnic, 2013).

One of the provided MP information of radar is the specific differential phase shift (K_{DP}), which is the difference between propagations constants for horizontal- and vertical- polarized radar pulses over a given range. This parameter is immune to attenuation and particle beam blockage. The other important parameters obtained are the Differential reflectivity (Z_{DR}) and coporal correlation (ρ_{HV}), which are related to the ratio and the shift correlation of horizontal reflectivity (Z_H) and the vertical reflectivity ((Z_V). These parameters have been applied to the QPE algorithms to give a better identification meteorological objects and the estimation of rain rate in Japan (Park et al., 2005).

Despite the potency, there are several disadvantages in the X-band radar performance. First, the maximum range is shorter than C-band and S-band radar. The X-band range is limited to 30-60km, while C- and S-band radar can cover up to maximum ranges of 200km or 300km. Second is related to the signal extinction area, which is the area where the received signal is below the receiver noise level occurs behind heavy rainfall areas (attenuation). These disadvantages can be a fatal flaw when extreme heavy rainfalls occur (Hirano et al., 2014).

In 2018, a breaking-record rainfall event happened in Western Japan to the Tokai region. Starting from 28 June to 8 July 2018, extreme rain in these regions and on 7 July 2018, the accumulated rain depth was 230mm (JMA, 2018). The event has resulted in more than 200 fatalities in 14 prefectures. Kagoshima is one of the prefectures in Kyushu, which has also received a more than 100mm rain depth in a day.

The event, which is known as the heavy rainfall of July 2018, is a perfect case to evaluate the performance of a small-compact X-MP radar in Kagoshima. The radar records every 1-minute rain rate within 100m mesh resolution, which can be useful for further study about the event and the impact in this area. However, the algorithm used to estimate the rain rate is unknown and confidential, which invites a question regarding its reliability (Putra et al., 2019; Syarifuddin et al., 2017). Comparing the rain rate values estimated by the radars to some common radar-rain rate algorithms, and their evaluation toward ground-based rain rate can give assurance for the further application of this radar.

This paper analyzes three different radar algorithms: Park et al. (2005), Marshall and Palmer (1948), and Bringi and Chandrasekar (2001), and their comparison to the manufactured radar-rain rate estimate (Furuno) and rain gauge measurement during the heavy rainfall of July event. The aim is to conclude the reliability of the radar-rain rate during the extreme rainfall event. At the same time, this work provides the spatial-temporal variability of the rain in Kagoshima especially in Sakurajima volcano during the analyzed period. This aspect is important as heavy rainfall is often associated with sediment disasters in the volcano area (Jenkins et al., 2015; de Belizal et al., 2013). The structure of the paper consists of an introduction, site location and methodology, result and discussion, and conclusion.

2. SITE LOCATION AND METHODOLOGY

2.1 Site location and data

The X-MP radar is deployed in Hirakawa, Kagoshima Prefecture (31.44 °N, 130.51 °E), 20 km from the city center, aiming to monitor the area of Mt. Sakurajima in the Kagoshima Bay by the sectoral Plan Position Indicator (PPI) scan mode. It operates at 2°, 5°, 10°, 15°, 20°, 25°, and 30° angular elevation levels, within 100m mesh spatial resolution and 1-min temporal resolution. Table 1 presents the specification of the deployed X-MP radar and Figure 1 shows the location and the area scanned by the X-MP radar in Kagoshima.

This study analyzed the estimated rain rate by Furuno and three radar parameters: Z_H, K_{DP}, and Z_{DR}, obtained at elevation angle 5°, from 6 July 2018 at 10:00 JST to 8 July 2018 at 9:00. Hourly ground-based rain rate provided by The Automated Meteorological Data Acquisition System (AMeDAS) of Japan Meteorological Agency (JMA), and atmospherics information from radiosonde data, provided by the University of Wyoming, are used to evaluate the reliability of the radar-based rain rate.

2.2 Data analysis

2.2.1 Pre-analysis

Pre analysis include the attenuation and ground clutter removal. The attenuation correction method done using the equations (1) and (2) proposed by Bringi and Chandrasekar (2001).

$$10\log Z_H(r) = 10\log Z_H' + \alpha\,[\Phi_{DP}(r) - \Phi_{DP}(0)] \quad (1)$$

$$10\log Z_{DR}(r) = 10\log Z_{DR}' + \beta\,[\Phi_{DP}(r) - \Phi_{DP}(0)] \quad (2)$$

where Φ_{DP} is differential phase, Z_H is corrected reflectivity factor, Z_H' is the attenuated reflectivity factor, Z_{DR} is corrected reflectivity factor, Z_{DR}' is attenuated reflectivity factor, calculated by the difference of differential phase of system Φ_{DP} (0) is and Φ_{DP} at a distance *(r).*

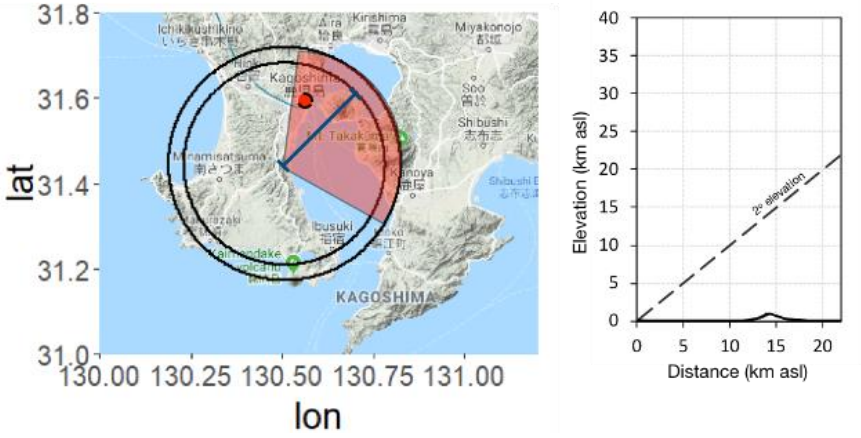

Figure 1. Left panel is the area scanned by sectoral PPI, presented by the red-shaded area. The red dot is the location of AMeDAS station. The inner circle shows the delineated area scanned by 30° elevation angle and the outer circle indicates the area scanned by the 2° elevation angle. Right panel is the 2° elevation angle (dash line) of radar scan extracted from the blue thick line in the left image and the topography of Sakurajima.

Table 1. Specifications of the X-MP radar WR 2100.

Parameter	Description
Transmitter	Solid state 200 W per channel (H,V)
Polarity	Dual polarimetric horizontal (H) and vertical (V)
Pulses	PRF 600-2500 Hz, Width 0.1-5.0 μs
Antenna	0.75 m ∅, 2.7° beam width
Antenna gain	33.0 dBi
Operating Frequency	9.47 GHz
Wavelength	3.3 cm
Scan mode	PPI, CAPPI, RHI
Maximum distance display	50 km
Maximum range fixed observation level	30 km
Data Output	Reflectivity Intensity – Z_H (dBZ), Differential reflectivity –Z_{dr} (dB), Doppler velocity – V_D(m . s^{-1}), Doppler velocity spectrum width - σ_{VD} (m . s^{-1}) Specific differential phase shift – K_{DP} (°km) Copolar correlation coefficient - ρ_{HV} Rainfall intensity – R (mm . h^{-1}), Cross polarization difference phase - Φ_{DP}

Source: Furuno WR 2100 operator manual handbook

Ground clutter in weather radar observations causes degradation of data quality and can lead to misinterpretation of radar echoes. In this study we removed all data that have lower than 0.9 coporal correlation, ρ_{HV} and Doppler velocity, V_D equals to 0.

2.2.2 Quantitative Precipitation Estimate by Radar

As a comparison to the given rainfall rate by the manufacture, QPE is done by three different methods proposed by Park et al. (2005), Bringi and Chandrasekar (2001), and Marshall Palmer (1948) in Eqs. (3)-(7), which is explained as follow

In Park et al (2005), when $K_{DP} \leq 0.3^{o}$ km^{-1}, the rain rate is given by Eq. (3)

$$R(Z_H) = c_1 {Z_H}^{a_1} \tag{3}$$

Otherwise, it is given by Eq. (4)

$$R(K_{DP}) = c_2 {K_{DP}}^{b_1} \tag{4}$$

Similarly, in Bringi and Chandrasekar (2001) for the same two-given condition, the algorithms of rain rate (R) respectively are given in Eqs. (5) and (6)

$$R(Z_H, Z_{DR}) = c_3 {Z_H}^{a_2} {Z_{DR}}^{b_2} \quad (5)$$

$$R(K_{DP}) = c_4 \left(\frac{K_{DP}}{f}\right)^{b_3} \quad (6)$$

Marshall and Palmer rain-radar algorithms is given by Eq. (7)

$$R(Z_H) = \left(\frac{Z_H}{200}\right)^{a_4} \quad (7)$$

here, a, b, and c are constants: a_1= 0.819, a_2=1.07, a_4= 0.625, b_1= 0.823, b_2 = -5.97, b_3=0.85, c_1= 7.07x10^{-3}, c_2=19.63, c_3= 3.93 x 10^{-3}, c_4= 129, f is radar frequency in GHz, equals to 9.47.

2.2.3 CAPPI interpolation

The Constant Altitude PPI (CAPPI) data is interpolated from a PPI scan mode to get the volumetric scan of the radar at 5º elevation angles. A uniform height mesh at 100 m increment is calculated by a linear approximation. For each known radar elevation (z) at the known values of (x,y) radar bin coordinate, their radar parameter values are interpolated linearly according to elevation change

$$\frac{(z-z_0)}{(n-n_0)} = \frac{(z_1-z_0)}{(n_1-n_0)} \quad (8)$$

$$R(n) = f(n_0) + \frac{f(n_1)-f(n_0)}{(n_1-n_2)}(n-n_0) \quad (9)$$

where n denotes bin coordinates or radar variables and f is the linear interpolation function of each set of coordinates and radar variables to the changes of altitude (z). Hence $p(n)$ is the approximate interpolated function of the coordinates and radar variables at a known n_1 and n_0 values in z_0 and z_1 elevation. Following the vertical/height interpolation, the horizontal interpolation for each radar parameter in their bin is done using the natural neighbor method.

CAPPI file has 100m horizontal mesh and 250 elevation levels, ranging from 500m to 25000m. Since CAPPI interpolation is the most consuming process in radar data management (Yang, et al., 2015), we bypass this process by using a linear regression model between a horizontal cross section of an interpolated three dimensional (3D) at 500m and the PPI scan of 5° elevation angle.

2.3 Evaluation.

A point-based correlation between all four rain radar estimates and rain recorded at a rain gauge in Kagoshima is done to evaluate the accuracy using linear regression model to compare the increase of rain depth.

3. Result and Discussion

3.1 Ground clutter removal and attenuation correction

An example of horizontal radar reflectivity factor, Z_H before and after the ground clutter removal and attenuation correction is presented in Figure 2. In the given example, this process gives more area with greater than 40 dBZ radar reflectivity and the removal of some ground clutter near the edge of radar blind-spot.

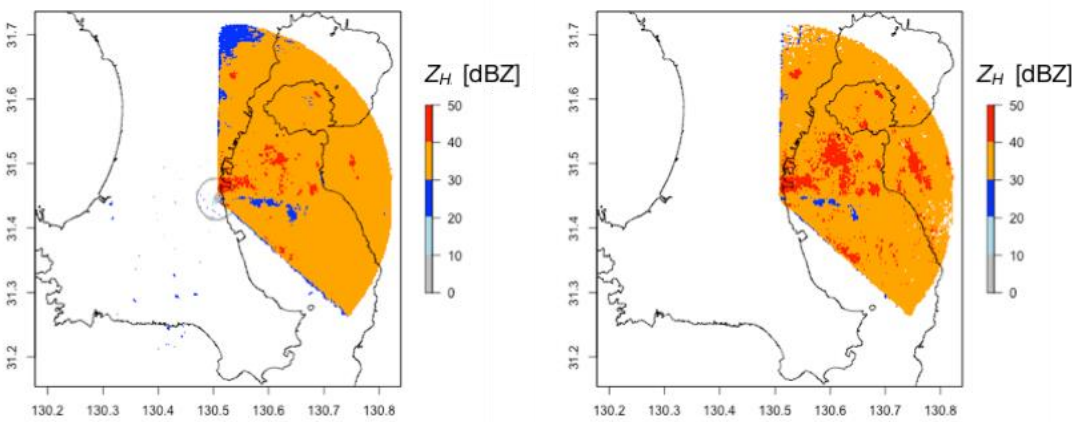

Figure 2 An example of reflectivity factor before pre-analysis by ground clutter removal and attenuation correction (left) and after pre-analysis (right) on 8 July 2018 (9:57 JST) using PPI scan mode at angular elevation 5°.

3.2 CAPPI interpolation

The best significant fitted model with $R^2 = 0.69$ is given by eq. (10)

$$R_{500} = 2.27 + 0.54PPI_2 \quad (10)$$

Hence, the extraction of CAPPI in our study reduces almost 50% of the PPI rain rate data.

3.3 Estimated rain rate

The high amount of rainfall received on 7 July 2018 is related to Baiu front circulation happened on 4-7 July, resulting in disastrous rains across western Japan. At the same time, there is also some meso-scale effects caused by low-pressure system developed near the Noto Peninsula at the Japan Sea (Kotsuki et al., 2019). Besides those factors, based on radiosonde data in Kagoshima (Figure 3), the atmospheric pressure and temperature condition from the period of rainfall analysis shows rapid temperature decrease to the value of lower than 0°C at about 5km-height and a slight instability of atmosphere occurred on 7 July at 550-500 HPa, at this 5km-height (Figure 3(c)). The instability of atmosphere would allow the rising of warm air mass to reach the condensation level, which creates more rainfall. The values of K_{index} during the period of observation are also higher than 30, which can be interpreted as there is a potency of wide scattered thunderstorm. During the period of observation, the radiosonde records a total of 267mm precipitable water.

Based on the vertical profile of Z_{DR} and ρ_{HV} in Figure 4, the melting layer is likely to occur at 3km-height, indicates by the decrease of ρ_{HV} and Z_{DR}. At this value, the ratio between horizontal and the vertical axis of raindrops may relatively equal, resulting in near to 0 values of Z_{DR}. However, the other meteorological objects such as hail and stone may interfere the reflectivity information, as the 0 ºC height is only 2km-height away, which then resulted in less than 0.2 ρ_{HV}.

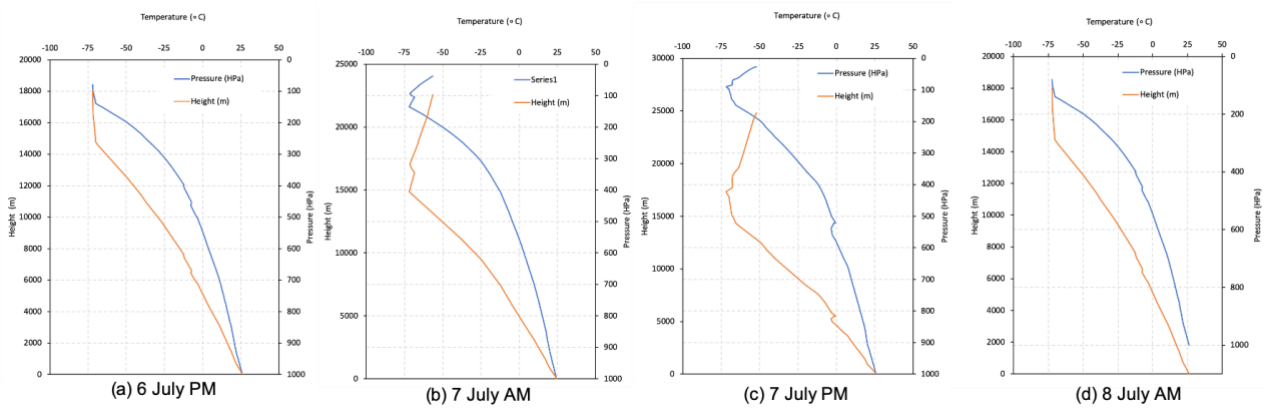

Figure 3. Vertical profile of temperature and pressure of the atmosphere measure by a radiosonde from 6 July PM (a), 7 July AM (b), 7 July PM (ac), and 8 July AM (d).

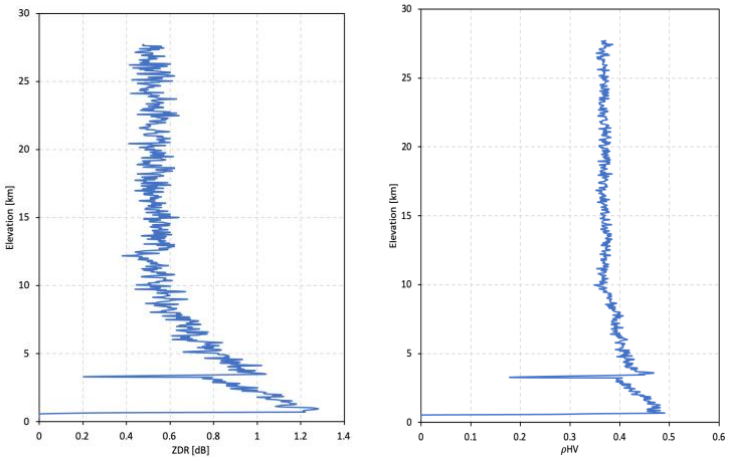

Figure 4. The vertical profile of Z_{DR} and ρ_{HV} on 7 July 2020 at 09:00 JST from the 5º elevation angle

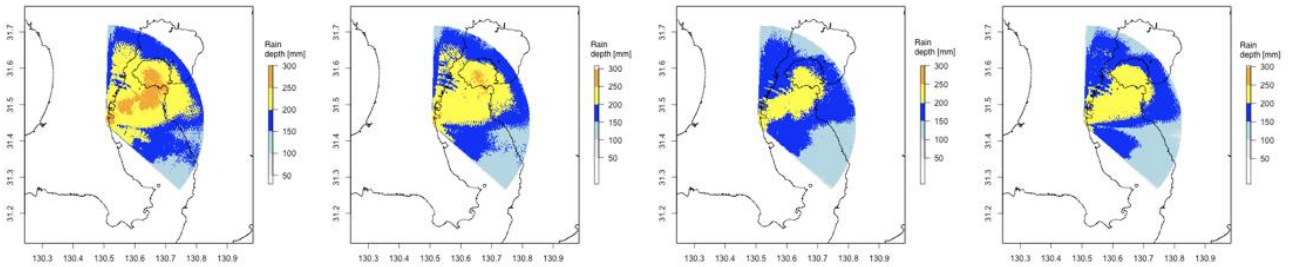

(a) Furuno (b) Park et al. (2005) (c) Bringi and Chandrasekar (2001) (d) Marshall and Palmer (1948)

Figure 5. Accumulated rain depth from the period of observation on 6 July 2018 to 8 July 2018 estimated by radar

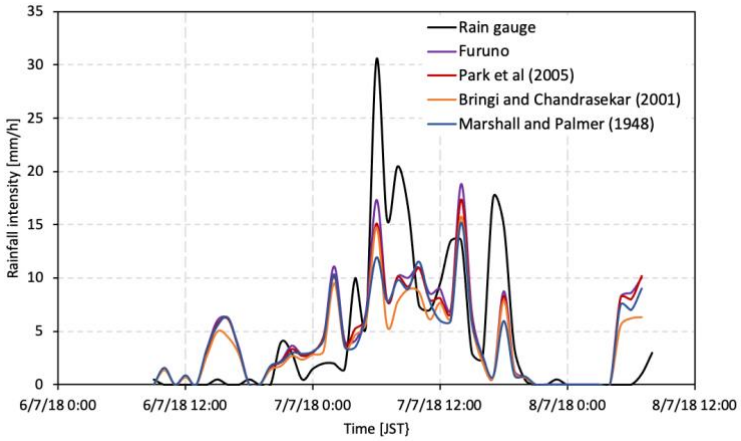

Figure 6. Point-based comparison of rainfall intensity from all four rain-radar algorithms and the ground-based rainfall at Kagoshima from AMeDAS. Rainfall values are extracted from the coordinate of AMeDAS station.

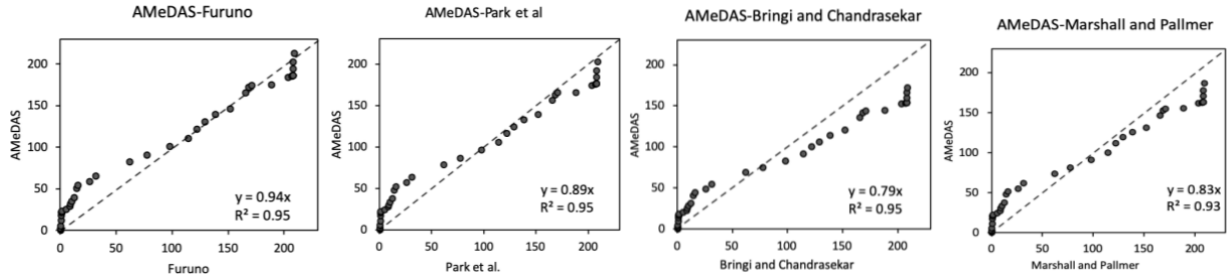

Figure 7. Correlation of rain depth increase of observed rainfall (AMeDAS) and radar-rainfall for the period of observation: 6 July 2018 (10:00 JST) – 8 July 2018 (9:00 JST)

The accumulated rain depth from CAPPI rain-rate at 500m elevation is presented in Figure 5. The Furuno rain rate gives the highest rain depth for the period of observation with more than 250mm depth at the southern part of Sakurajima. On the other hand, Bringi and Chandrasekar model, which used the combination of Z_{DR} and Z_H, gives the lowest area rainfall. These values are in agreement with the reported rain depth from the rain gauge at 210mm and the precipitable water of 267mm measured by radiosonde.

Comparing the point based given by the AMeDAS to the rain-rate extracted from radar resulted in a similar temporal fluctuation, but generally less intense rain rate, especially on 7 July 2018 (Figure 6). This result confirmed the previous founding about the tendency of this type of radar to underestimate the rain-rate which can be the results of representativeness errors or the interpolation process. The representativeness error is related to the point-based method of GR relationship by a raingauge, where the raingauge represents a much smaller area than the radar pixel (Habib et al., 2004).

The increase of error by the CAPPI interpolation process can be another reason for the underestimation of radar rain rate. Our analysis used the second elevation angle (5°) at the altitude range of 1 km to ≥22km, while the CAPPI was extracted at constant 500m elevation. As the CAPPI data reduced almost 50% of the rain rate estimated by the 5° elevation angle, then the rain rate from the PPI data was actually greater than the ground-based data. The greater intensity of the PPI scan mode may be related to the presence of hail and ice at altitude higher than the melting ratio (3km), which increases the reflectivity. Several studies also have found the increase of error according to the altitude increase. During the travel of raindrop, horizontal wind can have significant

effect, resulting in less correlation to the ground information (Tokay et al.,2009). Garcia-Vila et al. (2009) also compared the radar reflectivity data at altitudes of 200m and 500m and found that *Z–R* relationships could be derived very differently from each other.

Despite the difference in temporal rain-rate fluctuation, the accumulated rain depth shows a close correlation higher than 90%, and the given rain depth calculated from Furuno radar rain rate has a ratio of 1:0.94 to the increase of rain depth measured by the raingauge. The Park et al., algorithm gives the closest result to the Furuno rain rate, which indicates that the unknown Furuno algorithm used the combination of Z_H and K_{DP} to estimate the rain rate. The agreement in rainfall depth shows the applicability of radar data for hydrological purpose such as flood model, but certain improvement is still needed, in terms of the better interpolation model and the radar algorithms. Combining radar data from a single X-MP into an X-MP network may also increase the reliability of rainfall estimate.

4. CONCLUSIONS

An evaluation of an X-MP radar during the breaking record rainfall event on 6-8 July 2018 have been done in Kagoshima, Japan. The X-MP radar provides rain rate estimate, which is likely derived from the combination of reflectivity intensity Z_H and K_{DP}, similar to the Park et al., (2005) model. Despite giving lower rain rate estimate when being compared to the ground-based rainfall, in general the radar-based rain rate can follow the hourly rain rate fluctuation and gives a maximum of 1:0.94 ratio of rain depth accumulation. The spatial information provided by the radar data give an estimated rain depth at ~250 mm, at the southern part of Sakurajima Volcano. This value is in agreement with total precipitable water measured by radio sonde at 267 mm, and a total of 210 mm of rain depth measured by rain gauge.

ACKNOWLEDGMENTS

The authors thank Asst. Prof. Susana Jenkins from Nanyang Technological University, for her positive and valuable comments on this work. We are also indebted to Disaster Prevention Research Institute of Kyoto University for providing the WR 2100 X-MP radar data.

REFERENCES

Bringi V.N and Chandrasekar V. (2001). *Polarimetric Doppler Weather Radar: Principles and Applications*, Cambridge University Press, United Kingdom.

Ciach, G. J. and Krajewski, W. F. (2006). Analysis and modeling of spatial correlation structure of small-scale rainfall in Central Oklahoma, *Advances in Water Resources*, 29: 1450–1463

de Belizal, E., Lavigne, F., Hadmoko, D.S., Degai, J.P., Dipayana, G.A., Bachtiar, W.M., Marfai, M.A., Coquet, M., Le Mauff, B., Robi, A.K., Vidal, C., Cholik, N., and Aisyah, N. (2013). Rain-triggered lahar following the 2010 eruption of Merapi Volcano Indonesia. *Journal of Volcanology and Geothermal Research*. 261: 330-347.

Doviac, R.J and Zrnic, Z.S . (2013). Doppler Radar and Weather Observations: Second Edition. Dover Books on Engineering, Oklahoma.

Garcia-Vila P., Benarroch, A., Garcia, P., and Riera, J. (2009). Micro rain radar measurements of rainfall in Madrid. *3rd European Conference on Antennas and Propagation, EuCAP 2009*, 23–27 Mar 2009, Berlin, Germany.

Habib, E., Ciach, G.J., Krajewski, W.F. (2004). A method for filtering out raingauge re- presentativeness errors from the verification distributions of radar and raingauge rainfall. *Advances in Water Resources*, 27, 967–980.

Hirano, K., Maki, M., Maesaka, T., Misumi, R., Iwanami, K., and Tsuchiya, S. (2014). Composite rainfall map from C-band conventional and X-band dual-polarimetric radars for the whole of Japan, Extended abstract at *The Eighth European Conference on Radar in Meteorology qnd Hydrology*.

Jenkins, S.F., Phillips, J.C., Price, R., Feloy, K., Baxter, P.J., Hadmoko, D., de Belizal. E. (2015). Developing building-damage scales for lahars: application to Merapi volcano, Indonesia. Bulletin of Volcanology, 77:75

Kotsuki, S., Terasaki, K., Kanemaru, K., Satoh, M., Kubota, T., Miyoshi, T. (2019). Predictability of Record-Breaking Rainfall in Japan in July 2018: Ensemble Forecast Experiments with the Near-Real-Time Global Atmospheric Data Assimilation System NEXRA. *SOLA*. 15A: 1-7.

Marshall, J.S. and Palmer W.M. (1948). The distribution of raindrops with size. *J Meteor*. 5:154–166.

Park, S.G., Bringi, V.N., Chandrasekar, V., Maki, M, Iwanami, K. (2005). Correction of radar reflectivity and differential reflectivity for rain reflectivity for rain attenuation at X band: Part I: Theoretical and Empirical Basis. *Journal of Atmospheric and Oceanic Technology*. 22: 1621-1631.

Putra S, Ridwan B, Yamanoi K, Shimomura M, Sulistiyani, and Hadiyuwono D. (2019). Point-Based Rainfall Intensity Information System in Mt. Merapi Area by X-Band Radar. *Journal of Disaster Research*. 14: 80-89.

Syarifuddin M, Oishi S, Hapsari R, Legono D, and Iguchi M. (2017). Integrating X-MP radar data to estimate rainfall induced debris flow in the Merapi volcanic area. *Advances in Water Resources*, 110: 249–262.

Tokay, A., Hartmann, P., Battaglia, A., Gage, K., Clark, W., and Williams, C. (2009). A field study of reflectivity and Z–R relations using vertically pointing radars and disdrometers. *Journal of Atmospheric and Oceanic Technology*. 26: 1120 – 1134.

Yang, L., Jang B. J., Lim, S., Kwon K. C., Lee S. H., and Kwon K.R., (2015). Weather Radar Image Generation Method Using Interpolation based on CUDA. *Journal of Korea Multimedia Society*. 18(4): 473–482.